PERSPECTIVE OPEN ACCESS

Magnetically Driven Spinodal Decomposition as the Origin of Magnetic Softness of CoFeNi-Based Ferromagnetic High-Entropy Alloys

Andreja Jelen[1] | Pavol Priputen[2] | Michael Feuerbacher[3] | Anton Meden[4] | Janez Dolinšek[1,5]

[1]Jožef Stefan Institute, Ljubljana, Slovenia | [2]Faculty of Materials Science and Technology in Trnava, Slovak University of Technology in Bratislava, Trnava, Slovak Republic | [3]Ernst Ruska-Centre for Microscopy and Spectroscopy with Electrons, Forschungszentrum Jülich GmbH, Jülich, Germany | [4]Faculty of Chemistry and Chemical Technology, University of Ljubljana, Ljubljana, Slovenia | [5]Faculty of Mathematics and Physics, University of Ljubljana, Ljubljana, Slovenia

Correspondence: Janez Dolinšek (jani.dolinsek@ijs.si)

Received: 8 September 2025 | **Revised:** 19 February 2026 | **Accepted:** 24 February 2026

Keywords: high-entropy alloys | magnetic Gibbs free energy | soft ferromagnetism | spinodal decomposition

ABSTRACT

Many high-entropy alloys (HEAs) based on ferromagnetic (FM) 3*d* elements Co, Fe, and Ni are soft ferromagnets, possessing vanishingly small hysteresis loops. Their magnetic softness originates from specific nanostructure that is formed by spinodal decomposition, where nanodomains enriched in the FM elements Co, Fe, and Ni alternate with nanodomains enriched in either the nonmagnetic elements such as Cu or the antiferromagnetic 3*d* elements Cr and Mn. In nonmagnetic HEAs composed of the elements with markedly different atomic radii, spinodal decomposition is driven by the local volumes misfit of the two decomposed phases, each one gathering elements of similar atomic radii to minimize the lattice distortion energy. By a detailed analysis of the FM GaCoCrFeNi nanostructured HEA, where all five elements possess practically identical atomic radii, we argue that spinodal decomposition in the CoFeNi-based FM HEAs does not occur due to the local volumes misfit, but is magnetically driven via short-range FM order within the CoFeNi-rich clusters at temperatures far above the long-range FM transition, which reduces the magnetic Gibbs free energy G^{mag} sufficiently to stabilize the nanostructured state. The related FM AlCoCrFeNi nanostructured HEA behaves identically, supporting the magnetic origin of spinodal decomposition.

1 | Introduction

Many high-entropy alloys (HEAs) based on ferromagnetic (FM) 3*d* transition elements Co, Fe, and Ni are soft ferromagnets [1–20], possessing very narrow magnetization hysteresis loop, and in some cases also vanishing magnetostriction [6, 9, 16], where the FM material does not change its size and shape in an external magnetic field. The materials with this combination of magnetic properties are energy-efficient in alternating-current (ac) electromagnetic applications because the hysteresis losses are brought to minimum, while the vanishing magnetostriction implies that the material does not mechanically vibrate in an ac magnetic field and hence does not emit humming noise in the audio-frequency range that can be annoying to a human ear. Such materials are "supersilent" in ac applications such as transformer cores, stators of electromotors, magnetocaloric coolers, and magnetocaloric heat pumps. It has been conjectured that the magnetic softness and vanishing magnetostriction properties of the supersilent class of HEAs originate from their specific nanostructure that is formed by spinodal decomposition, where nanodomains enriched in the FM elements Co, Fe, and Ni alternate with nanodomains enriched in either the nonmagnetic elements such as Cu or the antiferromagnetic (AFM) 3*d* transition elements Cr and Mn [7, 9, 16]. An example is the equiatomic CoFeNiCuPd HEA with the face centered cubic (fcc) average structure and excellent magnetic softness, where the Co–Fe–Ni

nanodomains of 2–5 nm cross dimensions are intermixed with the Cu–Pd nonmagnetic 'nanospacers' of the same size [7]. In the AlCoCrFeNi HEA of average composition $Al_{28}Co_{20}Cr_{11}Fe_{15}Ni_{26}$, spinodal decomposition forms the nanostructure of an Al–Co–Fe–Ni (but Cr-free) FM matrix with a B2 structure (a chemically ordered body centered cubic – bcc), with highly Cr-enriched (but Al- and Ni-free) marginally magnetic spherical-like Co–Cr–Fe "nanoparticles" (NP) with an A2 structure (randomly chemically disordered bcc) and 64 nm average diameter, embedded in the matrix [13, 21]. A qualitatively similar, but hierarchically decomposed multi-length-scale micro- and nanostructure was observed also in the Al–Co–Cr–Fe–Ni HEAs of other compositions, where the actual decomposition depends sensitively on the concentration of the elements, the method of synthesis, and the thermal annealing conditions [22–24]. The same type of nanostructure was observed also in the FM bcc phase of the two-phase equiatomic GaCoCrFeNi supersilent HEA [16] (the second phase in this HEA is fcc, which is not nanostructured and is paramagnetic at room temperature, undergoing a spin glass transition at 6 K). Here also, the Ga–Co–Fe–Ni (Cr-free) FM matrix and the Cr-enriched Co–Cr–Fe marginally magnetic NPs of 10–30 nm diameter embedded in the matrix are formed by spinodal decomposition. A related spinodally decomposed nanostructure, but with the matrix/inclusions setting inverted (the matrix is A2, whereas the inclusions are B2) was also observed in the FM AlCoCrFeMn two-phase HEA of average composition $Al_{22}Co_{20}Cr_{21}Fe_{21}Mn_{16}$ [25], where the matrix is predominantly Cr–Fe–Mn, while the inclusions in the morphology of nanoplatelets of about 65 nm thickness and variable lateral extensions of the order of 500 nm are Al–Co rich. The nanostructure of the CoFeNi-enriched FM nanodomains, alternating with marginally magnetic Cu-enriched nanodomains was observed also in the supersilent HEA $AlCoFeNiCu_{2.5}$, which is composed of one bcc phase and two fcc phases with slightly different unit cell parameters [9]. A common feature of all the above described spinodally decomposed nanostructured FM HEAs is the fact that strong ferromagnetism originates from the nanodomains highly enriched in the FM elements Co, Fe, and Ni that do not contain significant amounts of the two AFM elements Cr and Mn, while the domains that are enriched in the Cr and/or Mn, and containing also small amounts of the Fe and Co, are weakly magnetic and do not contribute significantly to the ferromagnetism of these HEAs.

The magnetic softness and vanishing magnetostriction of the above-described nanostructured CoFeNi-based FM HEAs are both nanomagnetic phenomena, following the cognition that materials behave magnetically different from the bulk when at least one of their spatial dimensions is in the nanometer range. The nanometer-sized FM clusters of cross dimension D are magnetically single-domain particles and are coupled to each other across the boundaries by the exchange interaction. Since in a disordered HEA lattice, their FM axes are randomly oriented, the phenomenon of exchange-averaging of magnetic anisotropy takes place [26]. The effective magnetocrystalline anisotropy constant $\langle K \rangle$ of the material scales with the sixth power of the FM clusters' dimension, $\langle K \rangle \propto D^6$, decreasing rapidly towards zero for D in the sub-micrometer range. Since the coercivity scales with $\langle K \rangle$, the coercive field becomes vanishingly small for randomly oriented, exchange-coupled FM clusters of nanometer dimensions, leading to excellent magnetic softness. The origin of vanishing magnetostriction can be explained along the same lines. The CoFeNi-enriched FM nanodomains are small enough entities that the change of their size and shape in a magnetic field induced by the magnetostrictive strain are minute. In addition, due to the spatially random orientation of the domains' FM axes, the field-induced elongation/contraction of the nanodomains takes place in random directions, averaging out the net magnetostrictive strain to zero and resulting in a vanishing magnetostriction of the nanostructured material.

In this paper, we discuss the origin of spinodal decomposition in the CoFeNi-based FM HEAs, which leads to the above-described specific nanostructure that yields magnetic softness and vanishing magnetostriction of the materials. We argue that the spinodal decomposition must be magnetically driven, a phenomenon which has not been considered in literature as yet in the context of FM HEAs, to the best of our knowledge.

2 | Spinodal Decomposition in HEAs

Spinodal decomposition is a mechanism by which a system of two or more components in a metastable state spontaneously separates into two stable phases [27–29]. The decomposition does not require nucleation, but happens in the absence of a thermodynamic barrier to phase separation and is purely diffusion driven. Spinodal decomposition is an isostructural chemical decomposition (without change of the crystal symmetry), where each of the two coexisting phases is rich in one species and poor in the other. The two distinct phases start growing in any location uniformly throughout the volume, resulting in a nanoscale composition modulation over the entire crystal, while the lattice remains coherent among adjacent spinodal regions, at least in the early stages of the transformation. For most crystalline solid solutions, there is a variation of lattice parameters with the chemical composition, but if the lattice is to remain coherent in the presence of composition modulation, mechanical work has to be done to strain the rigid lattice structure. This involves the formation of elastic compressive or tensile coherency stresses at the borders between the nanoscale-dispersed spinodal regions, the magnitude and direction of which depend on the local volume misfit.

2.1 | Local-Volumes-Misfit Driven Spinodal Decomposition in the Nonmagnetic HfNbTaZr

An example of a spinodally decomposed solid solution, induced by the volume misfit of the two decomposed phases formed from otherwise well miscible components is the equiatomic four-component bcc HEA $Hf_{26}Nb_{25}Ta_{25}Zr_{24}$ [30, 31]. In the as-cast state of this nonmagnetic alloy, the four elements mix homogeneously on both the micrometer- and the nanometer scale, owing to the fact that the binary mixing enthalpies ΔH^{ij}_{mix} of any pair i,j of the elements are close to zero (between 0 and 4 kJmol^{-1} [32, 33]). Upon thermal annealing, a specific nanostructure develops in the form of a three-dimensional rectangular grid of Hf- and Zr-enriched interconnected planar clusters with spacing in the range 7–15 nm, while the matrix is enriched in Nb and Ta (Figure 1).

Both spinodally decomposed phases keep the bcc symmetry, but their unit-cell parameters differ significantly, $a_L = 3.48$ Å and $a_S = 3.37$ Å (with L and S standing for "larger" and "smaller"), leading to a difference in the unit cell volumes of $(a_L^3 - a_S^3)/a_S^3 = 10\%$.

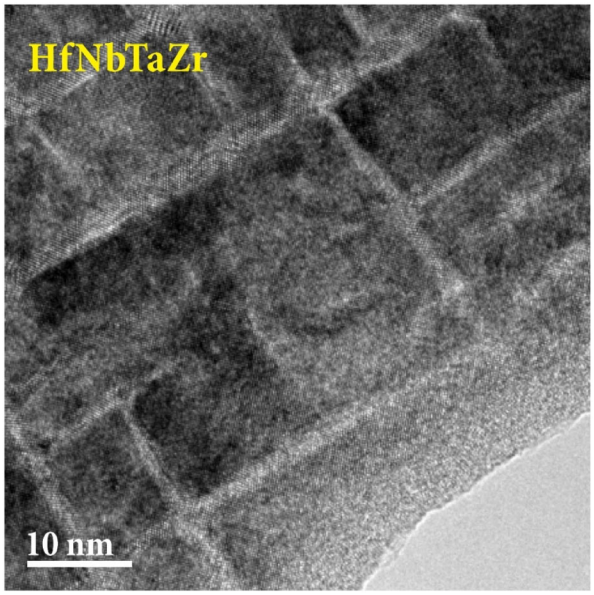

FIGURE 1 | HR-TEM bright-field image along the [100] zone axis of the $Hf_{26}Nb_{25}Ta_{25}Zr_{24}$ bcc HEA (reprinted from [31] with permission of Elsevier, 2017). The light-gray planar clusters are Hf, Zr-enriched, while the darker matrix is Nb, Ta-enriched.

The prime reason for the spinodal decomposition are the different atomic radii because the elements Hf ($r_{Hf} = 1.58$ Å) and Zr ($r_{Zr} = 1.60$ Å) are "large", while the elements Ta ($r_{Ta} = 1.43$ Å) and Nb ($r_{Nb} = 1.43$ Å) are "small" [32]. For the as-cast solid solution state with homogeneously dispersed elements, the atomic-size-difference (geometric) parameter $\delta = 100[\sum_{i=1}^{4} c_i(1 - r_i/\bar{r})^2]^{1/2}$ amounts to 5.3% (here c_i is the concentration of the component i and $\bar{r} = \sum_{i=1}^{4} c_i r_i$ is the composition-averaged atomic radius), whereas for the two spinodally decomposed phases, the δ values are reduced drastically. Assuming equiatomic binary compositions, we obtain $\delta = 0.6\%$ for the Hf Zr planar clusters and $\delta = 0.0\%$ for the NbTa matrix. By clustering together the larger Hf and Zr atoms on one side and the smaller Ta and Nb atoms on the other side, the lattice strain energy (electrostatic in origin) is strongly reduced inside the nanoscale-dispersed spinodal regions, at the expense of the smaller strain energy increase at the boundaries between these regions due to their different bcc lattice parameters a_L and a_S. The larger unit cell edge a_L refers to the Hf, Zr-enriched planar clusters, while the smaller one a_S refers to the Nb, Ta-enriched matrix.

2.2 | Magnetically Driven Spinodal Decomposition in FM HEAs

While the geometric lattice distortion (resulting in the local volumes misfit) is the prime reason for the spinodal decomposition in nonmagnetic multicomponent solid solutions composed of the elements with significantly different atomic radii, this may not be the case for the CoFeNi-based FM alloys with almost equal atomic radii. Such situation appears in the equiatomic GaCoCrFeNi HEA, which is FM below the Curie temperature $T_C = 725$ K, showing the combination of magnetic softness and vanishing magnetostriction (i.e., the supersilence property) [16]. The atomic radii of all five constituting elements are about the same, $r_{Ga} = 1.24$ Å, $r_{Co} = 1.25$ Å, $r_{Cr} = 1.25$ Å, $r_{Fe} = 1.26$ Å, and $r_{Ni} = 1.25$ Å [32], so that the atomic-size-difference parameter of a single-phase random solid solution would be minute, $\delta = 0.5\%$. This suggests that the lattice distortion due to unequal atomic radii cannot play a decisive role for the nanostructure formation in the bcc phase of this two-phase alloy, where the Ga–Co–Fe–Ni (Cr-free) FM matrix and the Cr-enriched Co–Cr–Fe weakly magnetic NPs are formed by spinodal decomposition. Hence, another mechanism must be the prime driving force for the spinodal decomposition in the GaCoCrFeNi HEA. In the following, we argue that the spinodal decomposition in this HEA, as well as in other CoFeNi-based FM HEAs is predominantly driven by the magnetic part of the Gibbs free energy.

The role of the magnetic Gibbs free energy G^{mag} in the phase equilibria of magnetic systems is well established [34–36]. The enthalpy can be lowered significantly by the specific form of spin ordering (FM, AFM, ferrimagnetic, etc) and the effect can be sufficiently large to cause fundamental changes in structure. The energy of a magnetic transformation often exceeds the one released by ordinary phase transformations. Many important phase changes are associated already with the magnetic short-range order (SRO) at temperatures much above the temperature where the magnetic long-range order sets in. The changes in phase equilibria directly attributable to G^{mag} are (1) a marked change in solid solubility, (2) a distortion of miscibility gaps (the Nishizawa horn), (3) a continuous transition between first- and second-order transformations, (4) stabilization of metastable phases by the magnetic Gibbs free energy contribution, (5) magnetic effects on the stacking-fault energy, (6) the relation between microstructure and phase diagram in magnetic alloys, and (7) magnetically induced chemical ordering of atoms in a crystal. In addition to the multicomponent alloys, the magnetic Gibbs free energy can be sufficiently large to affect fundamental structural changes also in unary systems. A well-known example is the allotropy of Fe [34], where the magnetic SRO plays a decisive role in the phase transformations already above the long-range FM transition that takes place at $T_C = 1043$ K. The high-temperature phase of Fe is bcc δ-Fe, which at 1665 K undergoes a transition to the more close-packed fcc γ-Fe. Both of these phases are paramagnetic at these elevated temperatures, but the onset of ferromagnetism in the bcc phase causes this phase to reappear at 1184 K as α-Fe. The thermodynamic effect due to the magnetic SRO is sufficient to cause re-appearance of the bcc phase. At $T = 0$ K, the magnetic enthalpy is about 9000 $Jmol^{-1}$, which is an order of magnitude larger than that involved in the high-temperature δ–γ and γ–α phase transformations (the latent heats of the transformations are about 1090 and 940 $Jmol^{-1}$, respectively).

3 | Structure and Nanostructure of the XCoCrFeNi (X = Al, Ga) HEAs

In the following, we consider the magnetic origin of spinodal decomposition in the CoFeNi-based FM HEAs by a detailed analysis of two closely related HEAs of the formula XCoCrFeNi with X = Al or Ga, which show qualitatively identical nanostructure [13, 16, 21]. Both Al and Ga elements belong to the group 13 of the periodic system, so they are isoelectronic from the valence-electrons point of view. Al possesses large negative binary mixing enthalpies with all four magnetic elements Co,

Cr, Fe, and Ni, while Ga possesses large negative mixing enthalpies with Co and Ni, but less negative with Cr and Fe (Table 1) [32, 33]. The important difference between Ga and Al is the considerably smaller atomic radius of Ga ($r_{Ga} = 1.24$ Å) [32], which is practically the same as the radii of the magnetic 3*d* elements (all about 1.25 Å), as compared to the larger atomic radius of Al ($r_{Al} = 1.43$ Å). For the random mixing of elements in a solid solution, the geometric lattice distortion would be large in the AlCoCrFeNi, while it would be essentially absent in the GaCoCrFeNi.

The crystal structure, microstructure, and nanostructure of the HEAs with nominal compositions in at.% $Al_{28}Co_{20}Cr_{11}Fe_{15}Ni_{26}$ (in the following conveniently abbreviated as HEA-Al) and $Ga_{20}Co_{20}Cr_{20}Fe_{20}Ni_{20}$ (HEA-Ga) were studied in detail before and the results are reported in two recent publications (ref. [13] for the HEA-Al and ref. [16] for the HEA-Ga). The HEA-Al material was grown by the Czochralski method and the details of synthesis and characterization by X-ray diffraction (XRD), scanning electron microscopy (SEM), energy-dispersive X-ray spectroscopy (EDS) and scanning transmission electron microscopy (STEM) can be found in refs. [13, 21], whereas the HEA-Ga material was prepared by induction melting, with the synthesis and characterization details given in ref. [16]. In the following we revisit the already published results and discuss them in a comparative way.

3.1 | Characterization of the XCoCrFeNi (X = Al, Ga) HEAs by XRD and SEM

Based on XRD, the HEA-Al is a bcc-phase material with the unit cell parameter $a = 2.875$ Å [13], while the HEA-Ga is a two-phase material, composed of a 56 wt.% fraction bcc phase with $a = 2.888$ Å and a 44 wt.% fraction fcc phase with $a = 3.623$ Å [16]. The SEM backscattered-electron (BSE) image of the HEA-Al is shown in Figure 2a, revealing the absence of microstructure on the SEM spatial scale.

TABLE 1 | Binary mixing enthalpies (in kJmol^{-1}) for unlike atomic pairs constituting the XCoCrFeNi alloys with X = Al or Ga [32, 33].

$_{24}$Cr	−1	−4	−7	−1	−10
−1	$_{26}$Fe	−1	−2	−2	−11
−4	−1	$_{27}$Co	0	−11	−19
−7	−2	0	$_{28}$Ni	−15	−22
−1	−2	−11	−15	$_{31}$Ga	
−10	−11	−19	−22		$_{13}$Al

The chemical composition determination by SEM-EDS point analysis has yielded the average composition $Al_{28}Co_{21}Cr_{12}Fe_{15}Ni_{24}$ (in at.%, rounded to first integers) that is very close to the nominal composition. The SEM-EDS elemental maps (Figure 3a) demonstrate homogeneous distribution of all five elements on the micrometer scale. The SEM BSE image of the HEA-Ga is shown in Figure 2b. A two-phase microstructure of dark inclusions in a light matrix is evident on a 100-µm scale, where the dark phase is fcc, while the light phase is bcc. The average SEM-EDS compositions of the two phases obtained via the point analysis are $Ga_{24}Co_{18}Cr_{18}Fe_{18}Ni_{22}$ for the bcc (light) phase and $Ga_{15}Co_{22}Cr_{23}Fe_{23}Ni_{17}$ for the fcc (dark) phase. The bcc phase is enriched in Ga and Ni (and depleted in Co, Cr, and Fe) with respect to the fcc phase. The SEM-EDS elemental maps (Figure 3b) reveal that within each phase, the elements are distributed quite homogeneously on this spatial scale.

3.2 | Nanostructure of the XCoCrFeNi (X = Al, Ga) HEAs

The nanostructure was investigated by STEM imaging, while the local chemical compositions were determined by STEM-EDS point analysis and elemental mapping. For each sample, a lamella of about 50 nm thickness was prepared by the focused ion beam (FIB) using Ga ions. The use of a Ga beam did not affect the accuracy of the results obtained on the HEA-Ga sample, because a noticeable increase of the Ga concentration due to the Ga ion implantation during the FIB thinning process could be detected only in the top Pt protective layer.

The high-angle annular dark-field (HAADF) STEM images of the HEA-Al on two magnification scales are shown in Figure 4a.

On the STEM spatial scale, the nanostructure in the form of a matrix with dispersed spherical-like nanometer-size domains (conveniently denoted as nanoparticles) of different chemical composition than the matrix becomes evident. The NPs are quite uniform in size, having an average diameter $d = 64$ nm with a standard deviation $\sigma_d = 10$ nm (as determined from the image analysis using ImageJ software [37]). The composition of the NPs determined by STEM-EDS is about $Co_{19}Cr_{56}Fe_{25}$, whereas the composition of the matrix is about $Al_{28}Co_{25}Fe_{15}Ni_{32}$, signifying that the NPs are Cr-rich, but Al- and Ni-free, while the matrix is Cr-free. The high-resolution (HR) STEM image is presented in

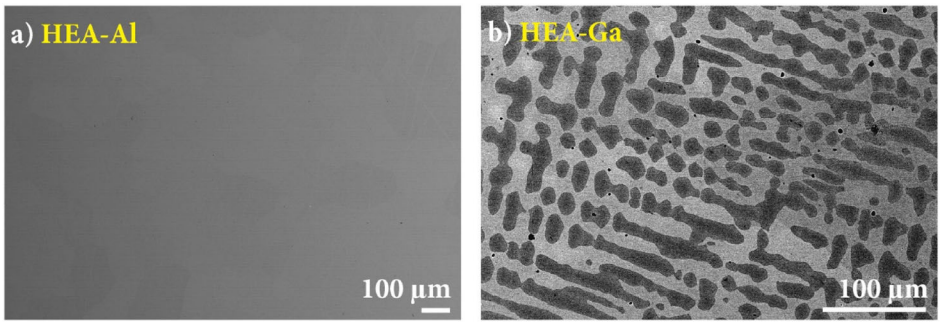

FIGURE 2 | (a) SEM BSE image of the bcc $Al_{28}Co_{20}Cr_{11}Fe_{15}Ni_{26}$ (HEA-Al) single-phase alloy. (b) SEM BSE image of the $Ga_{20}Co_{20}Cr_{20}Fe_{20}Ni_{20}$ (HEA-Ga) two-phase alloy (reprinted from [16] with permission of Elsevier, 2024). The light matrix is bcc, while the dark inclusions are fcc.

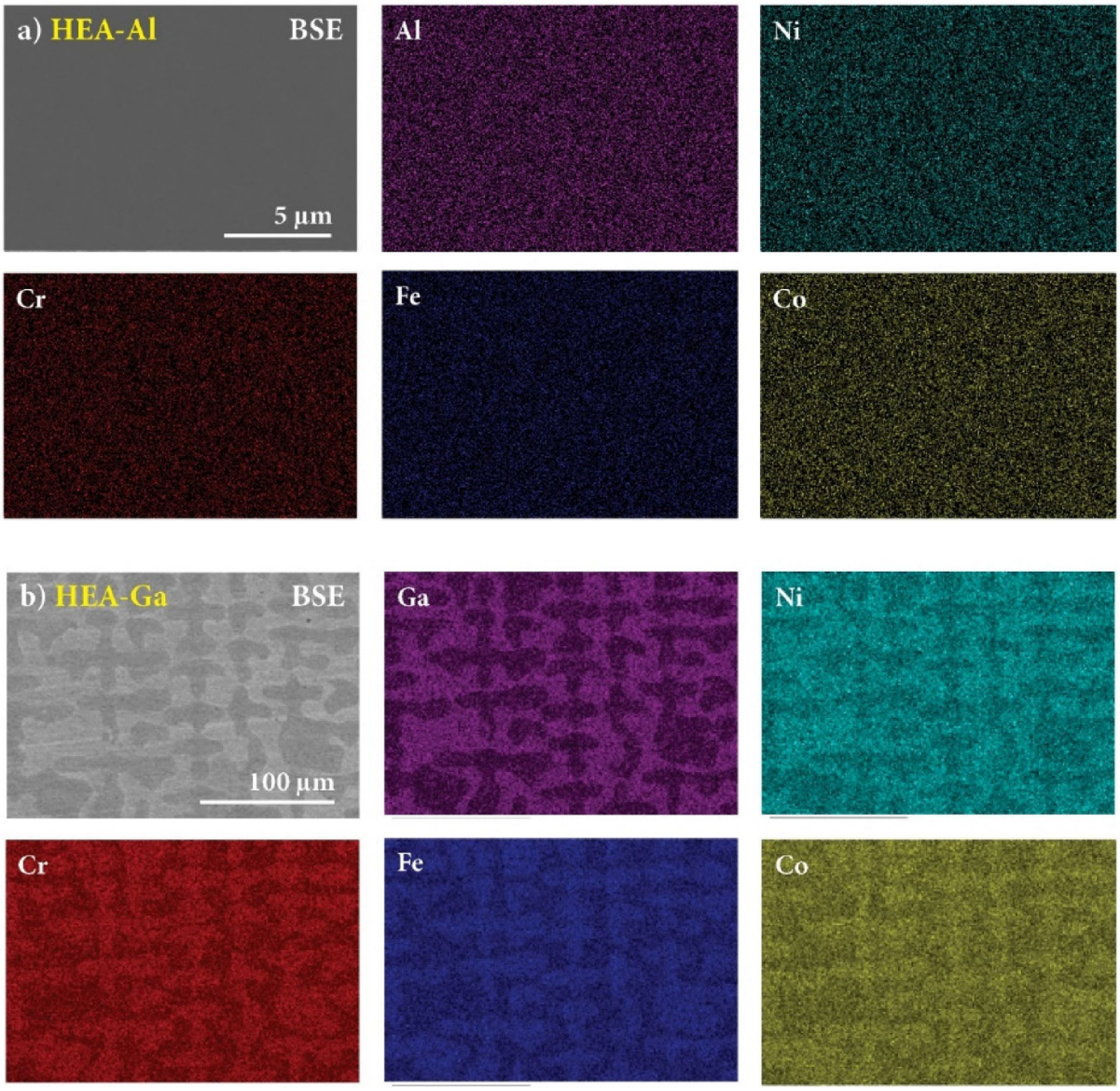

FIGURE 3 | (a) SEM-EDS elemental maps of the HEA-Al alloy. (b) SEM-EDS elemental maps of the HEA-Ga alloy (reprinted from [16] with permission of Elsevier, 2024).

Figure 5, revealing that the structure of the matrix is B2, because one of the B2 sublattices displays lower column intensity (i.e., the chemical contrast), while the NP' structure is A2.

The B2 matrix and the A2 NPs both possess the same unit cell parameter $a = 2.875$ Å. Figure 5 in addition shows that, in all crystal directions, the lattice planes of the NPs are perfectly congruent with those of the matrix, so that the lattices of the B2 and A2 phases are aligned and in perfect registry. The STEM-EDS elemental maps presented in Figure 6a show that the distribution of the elements in the Al–Co–Fe–Ni B2 matrix is uniform.

The A2 NPs, on the other hand, exhibit a core–shell structure (Figure 6b), where inside the core, the Co, Cr, and Fe elements are distributed quite uniformly, while the shell (a thin surface layer of about 2 nm thickness) is enriched in the Co and Fe elements. Since the B2 and A2 structures share a common Bravais lattice, but differ only in the chemical ordering of the elements, the above-described isostructural chemical decomposition is spinodal.

The nanostructure investigations of the two-phase HEA-Ga have shown the following features. The HAADF-STEM images of the bcc phase, presented on two magnification scales in Figure 4b, reveal that the nanostructure of this phase is qualitatively identical to that of the HEA-Al, consisting of the matrix and the spherical-like NPs of different chemical composition. The cross dimensions of the NPs are in the range 10–30 nm, hence significantly smaller than in the HEA-Al. The STEM-EDS composition of the NPs is about $Co_{13}Cr_{73}Fe_{14}$, while the composition of the matrix is about $Ga_{44}Co_{19}Fe_{14}Ni_{23}$, demonstrating that the NPs are highly enriched in Cr, but Ga- and Ni-free, while the matrix is Cr-free. The STEM-EDS elemental maps presented in Figure 7a confirm that the NPs are highly enriched in Cr and contain also some Fe and Co, while the matrix is Cr-free, but contains the other four elements. The question whether the crystal structure of the matrix and the NPs in the bcc phase of the HEA-Ga is in both cases A2, as suggested by the XRD pattern, or the situation is analogous to the bcc HEA-Al, where the matrix is B2, whereas

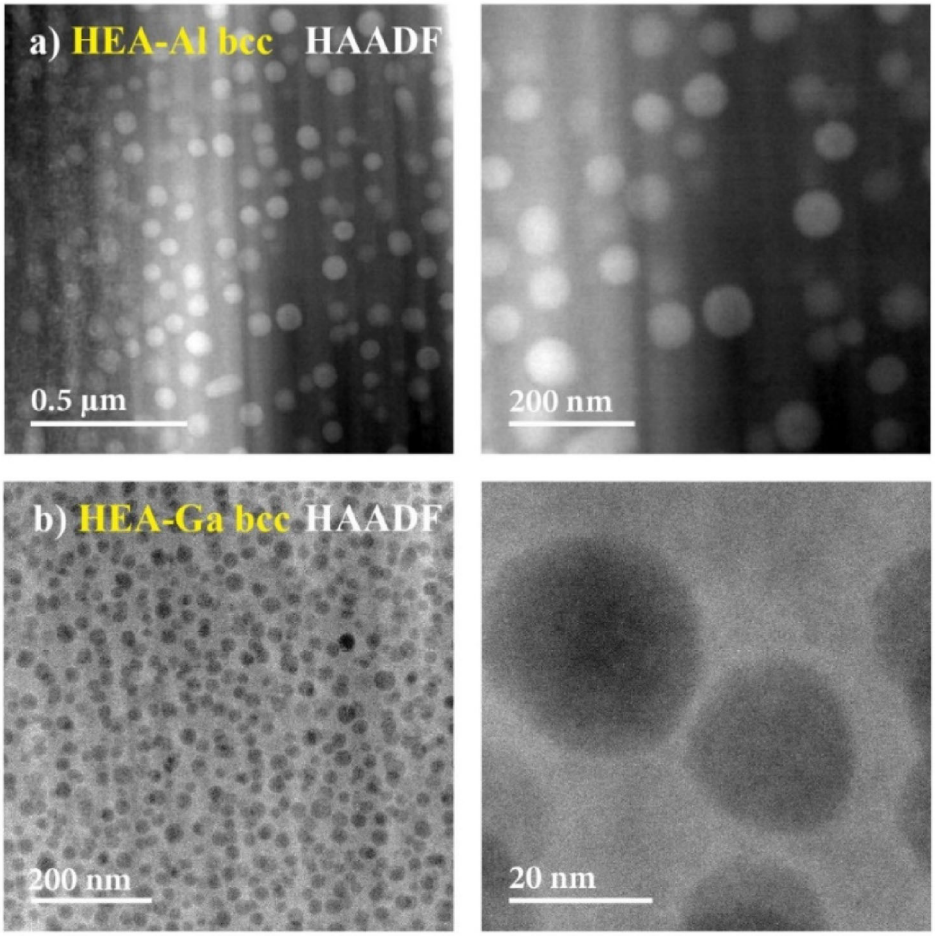

FIGURE 4 | (a) HAADF–STEM image of the HEA-Al bcc alloy (reprinted from [13] with permission of Elsevier, 2023). (b) HAADF–STEM image of the bcc phase in the HEA-Ga two-phase alloy (reprinted from [16] with permission of Elsevier, 2024). In each panel, the right image is a magnified part of the left image.

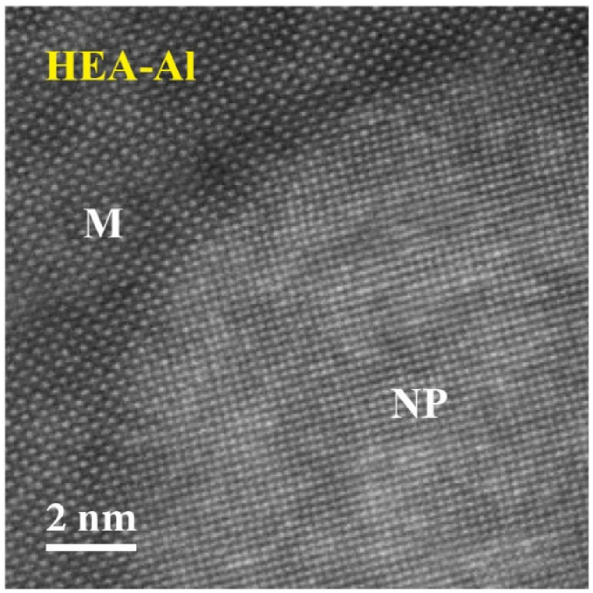

FIGURE 5 | HR STEM image of the HEA-Al alloy (reprinted from [21] with permission of Springer Nature, 2016). The nanoparticle (NP) has an A2 (disordered bcc) structure resulting in equal intensity on all atomic column positions. In contrast, the matrix (M) displays lower column intensity on one of the B2 (chemically ordered bcc) sublattices.

the NPs are A2, is not easy to answer unambiguously. The reason is that the atomic numbers of the Cr ($Z = 24$), Fe ($Z = 26$) and Co ($Z = 27$) elements that constitute the NPs, as well as the elements Fe, Co, Ni ($Z = 28$) and Ga ($Z = 31$) that constitute the matrix are so close that their atomic scattering factors do not differ sufficiently to produce clearly recognizable chemically sensitive reflections in the electron and XRD diffraction patterns, which would identify the B2 structure. Hence there exists a realistic possibility that the situations in the HEA-Ga and HEA-Al are identical also from the structural point of view, where the matrices are in both cases B2, while the NPs are A2. In any case, the isostructural chemical decomposition of the bcc phase in the HEA-Ga is spinodal.

The fcc phase in the HEA-Ga is not nanostructured according to the STEM imaging, but homogeneous also on the Nanometer scale. This is confirmed by the STEM-EDS elemental maps shown in Figure 7b, where a homogeneous distribution of all five elements on the nanometric scale is evident, demonstrating the absence of any nanostructure. Unlike the spinodally decomposed bcc phase, no spinodal decomposition takes place in the fcc phase of the HEA-Ga.

4 | Discussion

To argue that the magnetically driven spinodal decomposition is the dominant mechanism of the nanostructure formation in the

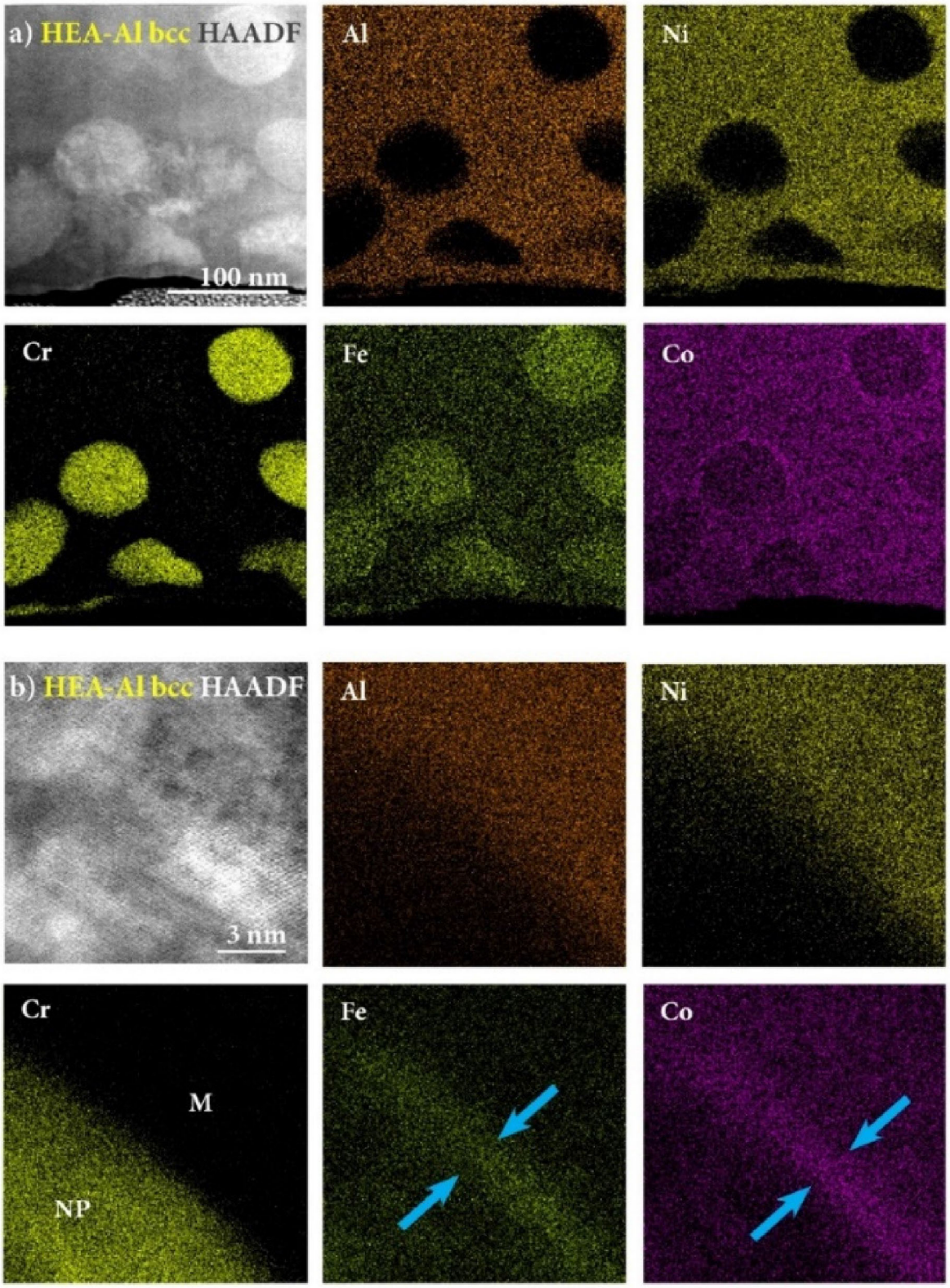

FIGURE 6 | (a) STEM-EDS elemental maps of the HEA-Al bcc alloy. (b) STEM-EDS elemental maps of the interface region between the A2 nanoparticle and the B2 matrix (both panels are reprinted from [13] with permission of Elsevier, 2023). The location of the Cr-rich nanoparticle (NP) is best identified in the chromium map, while the matrix (M) contains no Cr. An enrichment of the Co and Fe elements at the nanoparticle's surface in a shell of about 2 nm thickness is visible (marked by arrows in the Co and Fe maps), confirming the core–shell structure of the nanoparticle.

bcc phases of the above presented HEA-Al and HEA-Ga, we shall perform a qualitative discussion of phase(s) formation in these alloys. The discussion will be based on three main grounds: (1) the magnitude and sign of the binary mixing enthalpies between the elemental pairs that constitute the HEAs, where negative values cause attraction (binding) of the elements, while

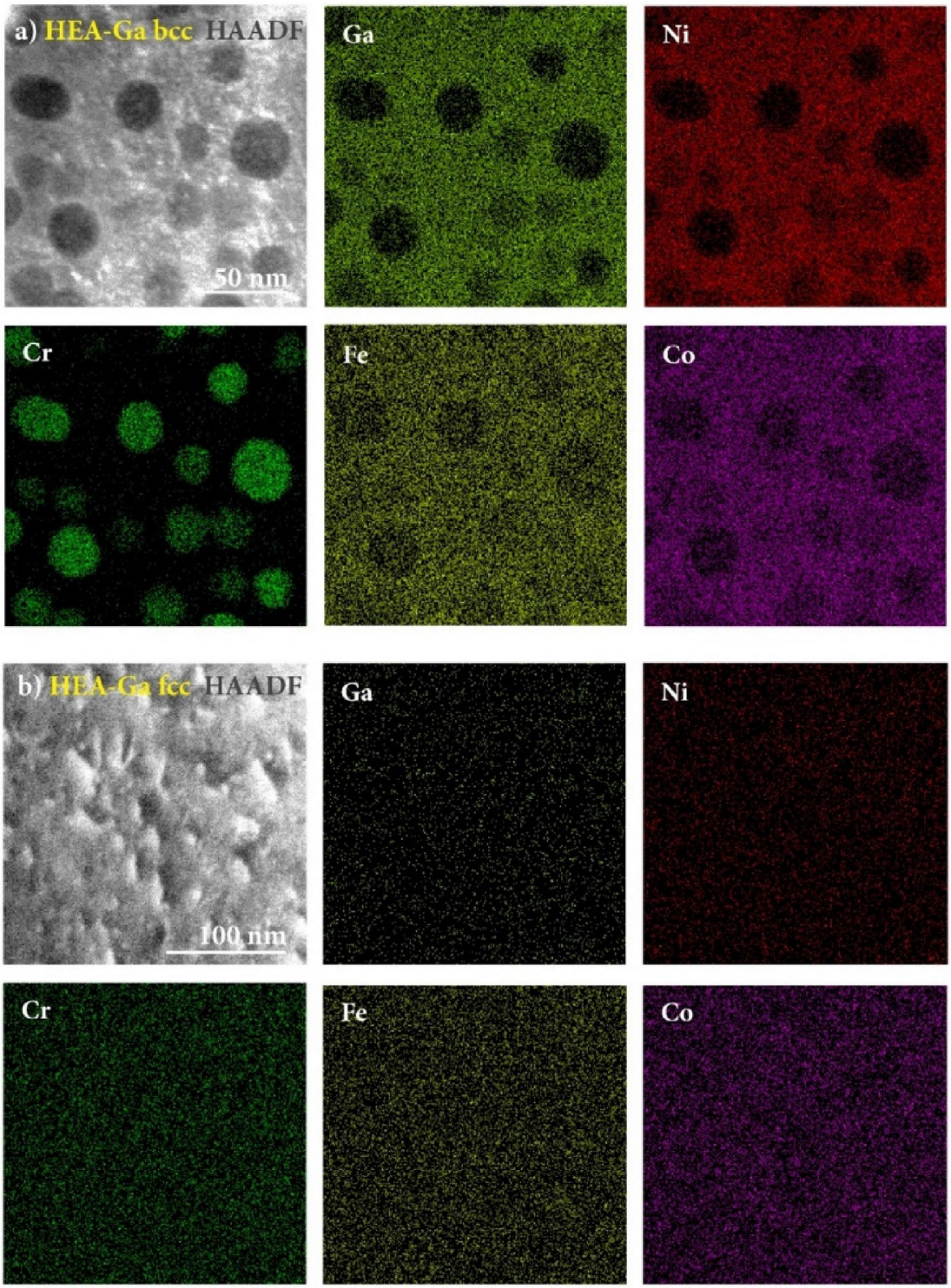

FIGURE 7 | STEM-EDS elemental maps of (a) the bcc phase and (b) the fcc phase in the HEA-Ga two-phase alloy (both panels are reprinted from [16] with permission of Elsevier, 2024).

positive values cause their repulsion; (2) the cognition that the phase formation in HEAs is governed more by the binary constituent pairs, which evolve first rather than the individual elements [38]; and (3) different preference for spin alignment (parallel or antiparallel) of the FM elements Co, Fe, and Ni and the AFM Cr to the spins of their neighbors, which affects the magnetic Gibbs free energy. Following the criteria (1) and (2), the parent crystal structure of the alloy will be determined predominantly by the binary pairs with the highest ordering energy (provided they are present in large enough amounts), into

which other elements dissolve subsequently due to their chemical compatibility and the mixing-entropy effect. As to the criterion (3), we shall use the presumption that in a metallic environment, the spins of the magnetic elements distributed on a chemically disordered lattice are coupled by the indirect exchange interaction via the conduction electrons and the magnetic state is exchange dominated, because random local magnetic anisotropy in 3*d* magnetic alloys is generally too weak to pin the magnetization direction at the atomic scale [39]. We shall further adopt the results of *ab initio* calculations performed for the Cantor alloy CoCrFeMnNi, which have predicted that the pairs of like and unlike FM neighbors (Co–Co, Fe–Fe, Ni–Ni, Co–Fe, Co–Ni, and Fe–Ni) show preference for a parallel (FM) spin alignment, while the spins of the Cr–Cr pairs and the unlike pairs of Cr with the Co, Fe, and Ni align antiparallel (AFM) [40, 41].

4.1 | Magnetically Driven Spinodal Decomposition in the bcc Phase of GaCoCrFeNi

We begin with the two-phase HEA-Ga. The macroscopic partitioning of the alloy with the nominal composition $Ga_{20}Co_{20}Cr_{20}Fe_{20}Ni_{20}$ into the fcc phase (44 wt.%) of the SEM-EDS average composition $Ga_{15}Co_{22}Cr_{23}Fe_{23}Ni_{17}$ and the bcc phase 56)wt.%) of the average composition $Ga_{24}Co_{18}Cr_{18}Fe_{18}Ni_{22}$ can be explained by considering the binary pairs. The pair with the most negative binary mixing enthalpy (the strongest attraction) is GaNi ($\Delta H_{mix}^{GaNi} = -15\,\mathrm{kJmol^{-1}}$, see Table 1), where the GaNi binary alloy crystallizes in a B2 structure. The GaCo ($\Delta H_{mix}^{GaCo} = -11\,\mathrm{kJmol^{-1}}$) also crystallizes in B2, while the GaFe ($\Delta H_{mix}^{GaFe} = -2\,\mathrm{kJmol^{-1}}$) and GaCr ($\Delta H_{mix}^{GaCr} = -1\,\mathrm{kJmol^{-1}}$) both crystallize in a rhombohedral structure with the space group $R\bar{3}m$. Upon cooling the GaCoCrFeNi melt, the first-to-form pair is GaNi that favors the B2 structure as the parent structure of the alloy. The B2 phase (observed experimentally as bcc, as argued in the chapter 3.2.) nucleates randomly in the parts of the melt with enriched concentrations of the Ga and Ni elements, while in the Ga, Ni-poorer parts, the fcc phase nucleates. The reason why the second phase is of the fcc symmetry cannot be explained by qualitative means because this is related to the electrostatic potential energy and the mixing entropy of this phase with respect to the competing phases. The bcc and fcc phases that develop in the HEA-Ga obviously possess very similar Gibbs free energies, depending sensitively on the concentrations of the constituent elements. The SEM-EDS average compositions of the bcc and fcc phases indicate that the amounts of the Ga and Ni elements in the bcc phase ($c_{Ga} + c_{Ni} = 46$ at.%) are sufficiently large that the GaNi first-to-form pairs determine the parent structure of this phase, while they are not large enough ($c_{Ga} + c_{Ni} = 32$ at.%) to prevail in the fcc phase. It is worth mentioning that the formation of the bcc and fcc phases on the macroscopic scale is in no relation to the magnetic Gibbs free energy G^{mag}.

The nanostructure formation in the bcc phase that consists of the highly Cr-enriched, but Ga- and Ni-free NPs of the STEM-EDS composition $Co_{13}Cr_{73}Fe_{14}$, embedded in a Cr-free matrix of the composition $Ga_{44}Co_{19}Fe_{14}Ni_{23}$, can be explained in the following way. The composition of the matrix can also be written as $Ga_{44}(Co, Fe,Ni)_{56}$, so that about half of the atoms are Ga and the other half are Co, Fe, and Ni. This indicates the approximate phase stoichiometry $Ga_{50}(Co, Fe,Ni)_{50}$, supporting the B2 structure of the matrix (favored by the GaNi first-to-form pairs), where one site of the unit cell is occupied by Ga, whereas the three FM elements Co, Fe, and Ni randomly populate the second site of the B2 unit cell. Random mixing of the elements Co, Fe and Ni at one site is supported by their close-to-zero binary mixing enthalpies ($\Delta H_{mix}^{CoFe} = -1\,\mathrm{kJmol^{-1}}$, $\Delta H_{mix}^{CoNi} = 0$ and $\Delta H_{mix}^{FeNi} = -2\,\mathrm{kJmol^{-1}}$). The fraction of the matrix relative to the fraction occupied by the NPs is determined by the amount of Ga and Ni elements present. The matrix absorbs all the Ga and Ni atoms and additionally also the appropriate portions of the Co and Fe atoms to satisfy the $Ga_{50}(Co, Fe,Ni)_{50}$ B2 stoichiometry. The rest of the atoms, consisting of all Cr atoms and the remaining amounts of the Co and Fe then form the NPs. Since there is no strongly bonded pair within these three elements (all binary mixing enthalpies are small, $\Delta H_{mix}^{CoFe} = -1\,\mathrm{kJmol^{-1}}$, $\Delta H_{mix}^{CoCr} = -4\,\mathrm{kJmol^{-1}}$, $\Delta H_{mix}^{FeCr} = -1\,\mathrm{kJmol^{-1}}$), there is no leading binary atomic pair that would dictate the parent structure of the NPs, which then appears as A2.

The fact that out of the four magnetic elements present in the alloy, the matrix contains only the three FM elements Co, Fe, and Ni, but no AFM Cr, is a magnetic effect, attributable to the magnetic Gibbs free energy G^{mag}. The reason why the B2 matrix composition is $Ga_{50}(Co, Fe, Ni)_{50}$ and not $Ga_{50}(Co, Cr, Fe, Ni)_{50}$ cannot be explained on the basis of binary mixing enthalpies. The weak attraction of Cr to Ga is about the same as that of Fe to Ga ($\Delta H_{mix}^{GaCr} = -1\,\mathrm{kJmol^{-1}}$ versus $\Delta H_{mix}^{GaFe} = -2\,\mathrm{kJmol^{-1}}$), so that this cannot be the reason for the exclusion of Cr, while keeping the Fe. Cr also shows moderate attraction to Ni ($\Delta H_{mix}^{NiCr} = -7\,\mathrm{kJmol^{-1}}$) and Co ($\Delta H_{mix}^{CoCr} = -4\,\mathrm{kJmol^{-1}}$), so that from this criterion, there is no obvious reason why Cr would not mix with the Co, Fe, and Ni to form the $Ga_{50}(Co, Cr, Fe, Ni)_{50}$ stoichiometry of the matrix. However, by excluding the AFM Cr and keeping the three FM elements Co, Fe, and Ni, the FM-type indirect exchange interactions are present in the matrix only, which consequently achieves long-range FM spin ordering below the Curie temperature $T_C \approx 725$ K [16]. By entering the FM state, the matrix efficiently lowers its magnetic Gibbs free energy G^{mag}, which adds to its thermodynamic stability against the competing phases. The presence of Cr that would be randomly mixed with the Co, Fe, and Ni would create AFM couplings of Cr with all of their neighbors (the Cr-containing like and unlike pairs), and the spin system would then possess mixed FM and AFM interactions, as characteristic for a spin glass-type magnetically disordered state. Due to the much smaller magnetization of the spin glass state as compared to the FM state, the magnetic stabilization effect of the structure via the G^{mag} would be much smaller, if any at all. By excluding the AFM Cr and keeping only the three FM elements Co, Fe, and Ni, the stabilization effect via the G^{mag} is the strongest. On the other hand, the Co–Cr–Fe NPs represent a system with mixed FM and AFM interactions, where there is no long-range spin ordering and the system remains paramagnetic down to low temperatures (perhaps exhibiting a spin glass-like spin freezing below 10 K), so that the magnetic stabilization effect is negligible.

The nanostructure of the HEA-Ga bcc phase starts to form below the melting temperature ($T_m \approx 1560$ K) of the as-solidified alloy via the magnetically driven spinodal decomposition. Thermal diffusion of atoms in the solid state is typically effective at temperatures between T_m and about $T_m/2$ [35, 42], i.e., between 1560

and 780 K in the present case, which is in the paramagnetic regime of the bcc phase with $T_C \approx 725$ K. The diffusion builds up short-range ferromagnetically ordered Ga–Co–Fe–Ni clusters, inside which the magnetic Gibbs free energy is sufficiently reduced to provide thermodynamic stabilization of the clusters. Upon cooling, the SRO FM clusters grow in size and become increasingly more interconnected, finally forming a continuous matrix that undergoes long-range FM ordering below T_C. Due to the random mixing of the Co, Fe and Ni elements that possess different atomic magnetic moments, the long-range FM-ordered state can be best characterized as a disordered FM state, consisting of small FM domains with distributed magnitudes of the domains' magnetic moments and randomly oriented directions of their FM axes. The Co–Cr–Fe NPs, on the other hand, do not undergo magnetic ordering and there is no strong magnetic contribution to their stabilization. The FM-type magnetic SRO in the Ga–Co–Fe–Ni clusters hence drives the spinodal decomposition in the bcc phase of the HEA-Ga. Here, it is worth recalling that due to the very similar atomic radii of all five elements constituting the HEA-Ga, the local-volume-misfit mechanism upon elements' clustering does not appear to play any significant role in the spinodal decomposition of this HEA.

4.2 | Magnetically Driven Spinodal Decomposition in the bcc AlCoCrFeNi

The nanostructure formation in the single-phase HEA-Al is analogous. The nanostructure again consists of a B2 Cr-free FM matrix that absorbs all the Al and Ni atoms (its STEM-EDS composition is about $Al_{28}Co_{25}Fe_{15}Ni_{32}$), while the embedded A2 NPs of composition $Co_{19}Cr_{56}Fe_{25}$ are Cr-rich, but Al, Ni-free. The first-to-form pair is AlNi ($\Delta H_{mix}^{AlNi} = -22\,\mathrm{kJmol^{-1}}$), followed by AlCo ($\Delta H_{mix}^{AlCo} = -19\,\mathrm{kJmol^{-1}}$), where both binary compounds possess the B2 structure. The parent structure of the matrix is hence B2, which is confirmed experimentally in Figure 5 by the chemically sensitive contrasts in the HR-STEM image (since the atomic scattering factor of Al ($Z = 13$) is different enough from those of the magnetic elements, the chemical contrast in the HEA-Al is clearly observed). It is worth mentioning that the stoichiometry of the HEA-Al matrix, which can also be written as $Al_{28}(Co, Fe,Ni)_{72}$ is significantly more distant from the exact B2 stoichiometry $Al_{50}(Co, Fe,Ni)_{50}$ than it is in the HEA-Ga. The reason is very likely the inaccuracy of the STEM-EDS measurement, because upon traveling through the matrix, the electron beam could have "touched" a NP hidden underneath in a 50-nm thick FIB lamella, resulting in an artificial enhancement of the concentrations of the Co and Fe elements that are present both in the matrix and in the NPs (a small concentration of Cr in the amount of 4 at.% was also detected in the matrix, see [13] for details). The possibility that the magnetic elements also replace some Al at its site in the B2 unit cell cannot be excluded as well. The A2 structure of the Co–Cr–Fe NPs in the HEA-Al follows from the same arguments as in the case of the HEA-Ga. In the absence of a leading binary atomic pair that would dictate the parent structure, no chemical ordering takes place and a chemically disordered A2 structure results. Despite the chemical and structural similarity of the NPs in the HEA-Al and HEA-Ga, there is one important difference. The NPs in the HEA-Al are significantly larger (average diameter of 64 nm with a standard deviation of 10 nm) than in the HEA-Ga (10–30 nm) and show a core–shell morphology with a 2-nm shell highly enriched in the Co and Fe with respect to the core, while the core–shell morphology was not detected for the smaller NPs in the HEA-Ga.

The nanostructure formation in the HEA-Al again proceeds via the magnetically driven spinodal decompositon. The magnetic SRO stabilizes the Al–Co–Fe–Ni FM clusters within the paramagnetic phase via the decrease of their magnetic Gibbs free energy G^{mag}. Upon cooling, the clusters grow into a continuous matrix that undergoes a transition to the long-range ordered FM state at $T_C \approx 390$ K [13]. The FM SRO in the Al–Co–Fe–Ni clusters hence drives the spinodal decomposition in the HEA-Al, while Cr is again excluded from the matrix because of its AFM coupling tendency in all Cr-containing like and unlike atomic pairs, which would result in a reduced magnetic stabilization effect via the G^{mag}.

The reason for the formation of the core–shell structure of the Co–Cr–Fe NPs in the HEA-Al can again be explained by the magnetic stabilization effect attributable to G^{mag}. In a recent TEM study, the spatially resolved magnetism of the related $AlCo_{0.5}Cr_{0.5}FeNi$ HEA, prepared by arc-melting, was studied on the nanometric scale by the methods of Fresnel mode of Lorentz TEM and off-axis electron holography [22]. This alloy also decomposes into the Al–Co–Ni-rich B2 matrix and the Co–Cr–Fe A2 inclusions, but the inclusions appear on three length scales, (i) coarse (average size 1–5 μm), (ii) medium-scale (50–150 nm), and (iii) fine-scale (<10 nm). The coarse and medium-scale inclusions both show a core–shell structure, where the shell is CoFe-rich, but contains almost no Cr, while the core is Cr-rich. The core and the shell both possess the A2 structure (in complete analogy to the NPs in the HEA-Al). The magnetic contrast in the TEM images taken at $T = 300$ K (in the FM state of the alloy) has revealed that the CoFe-rich shells are strongly FM relative to the inclusions' cores, supporting the hypothesis that the core–shell structure is also formed by the magnetically driven spinodal decomposition that provides its stabilization via the reduction of the magnetic Gibbs free energy G^{mag}.

Since the atomic radius of Al is significantly larger than the radii of the magnetic 3*d* elements, it seems at first glance that the local-volume-misfit mechanism of spinodal decomposition could play a more important role in the HEA-Al than it does in the HEA-Ga. However, the lattice distortion in the HEA-Al due to unequal atomic radii would be significant for a solid solution in which Al randomly mixes with the four magnetic elements at all sites of the unit cell. In the chemically partially ordered B2 structure of the HEA-Al matrix, the larger atom Al occupies one site of the B2 unit cell, while the other site is occupied by a mixture of the magnetic elements of smaller, but practically equal radii. In this case, there is no need for the lattice distortion (this would be strictly true for the exact $A_{50}B_{50}$ B2 stoichiometry), so that the local-volumes-misfit mechanism of spinodal decomposition in the HEA-Al is again expected to be ineffective with respect to the magnetically driven spinodal decomposition.

4.3 | Spin-Driven Chemical Ordering in the fcc Phase of GaCoCrFeNi

We comment also on the role of the magnetic Gibbs free energy on the formation of the fcc phase in the HEA-Ga. The fcc phase is not nanostructured, but all five elements are homogeneously

dispersed on the nanometric scale (see Figure 7b), revealing that spinodal decomposition does not take place in this phase. As already discussed in the chapter 4.1., the concentrations of Ga and Ni elements in the fcc phase are insufficient that the first-to-form GaNi pairs would dictate the parent structure to be B2. There is also no short-range clustering of the FM elements Co, Fe, and Ni in the fcc phase that would make the phase FM, but the three FM elements are randomly intermixed with the AFM Cr at the atomic level. Consequently, the FM and AFM spin couplings between the pairs of magnetic elements are randomly distributed over the system due to random positioning of the magnetic atoms in the lattice and the phase remains paramagnetic down to 6.7 K, where spin freezing into a spin glass phase was observed [16]. The occurrence of a spin glass phase (of a site-disordered type) provides indirect evidence of random mixing of the FM and AFM elements in the lattice at the atomic scale, without clustering of a particular subset of the elements. This feature can again be attributed to the stabilization effect via the magnetic Gibbs free energy G^{mag}, in this case to lowering of the G^{mag} by the magnetically induced chemical ordering of single atoms. Spin-driven chemical ordering of the Co, Cr, Fe, and Ni atoms in the fcc lattice was theoretically demonstrated before by *ab initio* calculations for the 4-component equiatomic fcc phase CoCrFeNi [43], and those results are qualitatively applicable also to the GaCoCrFeNi fcc phase because of the nonmagnetic nature of the fifth element Ga. The calculations were performed for fcc clusters containing either 24 or 120 atoms and the magnetic moments of the atoms were calculated. The results have shown that Cr has strong energetic preference for not sitting within its own 1st nearest-neighbor (1NN) shell, but escapes to the 2NN shell, because its moment becomes most negative when it is surrounded by FM neighbors only, while it becomes less negative when it has more Cr in the 1NN shell. The Co, Fe, and Ni, on the other hand, favor parallel (FM) arrangement of their positive moments when sitting in the 1NN shell. Chemical ordering (segregation) of Cr into the 2NN shell creates an alloyed $L1_2$ structure (a chemically ordered fcc), which leads to the reduction of the magnetic Gibbs energy G^{mag} and provides stability of the $L1_2$ structure, in competition with the chemically disordered fcc. These results are in line with the theoretical study of the relative energetics of mixing the AFM solute Cr into the FM solvent Fe in Fe–Cr alloys, showing that Cr solutes have an energetic preference to spatially separate in the FM host via the reduction of G^{mag} by avoiding sitting in their own 1NN [44]. Anticipating those results to the fcc phase of the HEA-Ga, we argue that the mechanism of magnetically induced chemical ordering of Cr is responsible for its spin glass behavior. The $L1_2$ chemically ordered superstructure was, however, not observed experimentally by XRD in the fcc phase of the HEA-Ga, and the reasons are very likely again the too close atomic scattering factors of the elements.

5 | Conclusions and Perspectives

By performing a thorough analysis of the nanostructure formation in the XCoCrFeNi (X = Al, Ga) HEAs, we have demonstrated the relevance of the magnetic Gibbs free energy G^{mag} in the phase equilibria of FM HEAs based on the 3*d* elements Co, Fe, and Ni. The FM bcc phase of these HEAs is nanostructured, where partitioning into the CoFeNi-rich FM matrix and the marginally magnetic Cr-rich NPs is formed by magnetically driven spinodal decomposition. The FM SRO within the X-Co–Fe–Ni clusters at temperatures much above the long-range FM transition efficiently lowers G^{mag} and provides magnetic stabilization of the FM clusters and therewith of the nanostructure. Theoretical analysis [43] suggests that the fcc phase, which is not nanostructured, is affected by the magnetic Gibbs free energy as well, causing magnetically driven chemical ordering of the elements on the atomic scale. Spin-driven chemical ordering of the Co, Cr, Fe, and Ni atoms in the fcc lattice pushes the AFM Cr into local environments where it is surrounded by the three FM neighbors Co, Fe, and Ni only, but avoids direct contacts to other Cr atoms. In this way, the partially chemically ordered fcc structure ($L1_2$-type) is stabilized by a reduction of G^{mag}, in competition with the chemically disordered fcc structure. The experimentally observed spin glass state of the fcc phase in the HEA-Ga supports this kind of partial chemical ordering.

The type of nanostructure found in the bcc phase of the XCoCrFeNi (X = Al, Ga) HEAs, formed by the magnetically driven spinodal decomposition leads to magnetic softness of the alloys via the exchange averaging of magnetocrystalline anisotropy to zero and to vanishing magnetostriction, which together define the supersilent class of FM HEAs [9, 16]. It is straightforward to consider that the magnetically driven spinodal decomposition could be the general principle underlying the magnetic softness of also other CoFeNi-based FM HEAs, with or without the addition of another magnetic (AFM) element Cr and/or Mn, as reported numerously in the literature [1–20]. The examples of almost perfectly magnetically soft FM HEAs containing only CoFeNi, but no AFM element, are the CoFeNiCuPd [7] and $AlCoFeNiCu_{2.5}$ [9].

The above performed analysis is qualitative, founded on (1) the binary mixing enthalpies, (2) the assumption that the phase formation is governed by the first-to-form binary pairs, and (3) the different energetic preference for spin alignment of the FM elements Co, Fe, and Ni and the AFM Cr to the spins of their neighbors. A more quantitative treatment of the nanostructure formation by the magnetically driven spinodal decomposition appears to be difficult. A semi-quantitative treatment by the calculation of phase diagrams (CALPHAD) method should in principle be possible because the magnetic Gibbs energy is included in the approach [34]. However, in a 5-component system like the investigated HEAs, it is difficult to properly partition the long-range and short-range magnetic orders to construct a suitable expression for the Gibbs free energy. The incorporation of the magnetic SRO is necessary because the nanostructure formation takes place in the paramagnetic phase, before the long-range FM order sets in. It is also not clear how to construct the magnetic enthalpy H^{mag} of a magnetically disordered state in a HEA because the exchange interactions are distributed continuously due to randomness in the lattice. Quantitative *ab initio* calculations of the nanostructure formation via the magnetically driven spinodal decomposition seem more appealing, but there emerges a question on how representative such calculations are for a realistic material. The calculations are typically performed on atomic clusters containing of the order of 100 atoms, while even the smallest NPs of 10 nm diameter in the nanostructured bcc phase of the HEA-Ga contain about 20,000 atoms.

Finally, we comment on the recently reported tailoring of magnetic properties in the FM FeCoNiMnCu HEA via spinodal

decomposition [45]. The key idea there was that Fe–Co enriched regions are formed, which have an expanded volume (relative to the unconstrained Fe–Co) due to coherency constraints imposed by the surrounding matrix, so that the spinodal decomposition is considered to be local-volumes-misfit driven. Since the Co and Fe atoms possess large magnetic moments that align parallel (according to the *ab initio* calculations for the Cantor alloy, the moment of Ni is much smaller [40, 41]), the Fe–Co enriched clusters in the paramagnetic phase are expected to possess strong FM SRO. It remains to be considered whether the magnetic Gibbs free energy G^{mag} plays an important role in the spinodal decomposition also in that case.

A related issue is the spinodal decomposition in the family of Fe-based alloys with the acronym alnico, which are in addition to Fe composed primarily of Al, Ni, and Co, but contain also Cu and sometimes Ti. The alnico alloys are FM and are commercially used as hard permanent magnets. After heat treatment, the alnico becomes a composite material, named also 'precipitation material', consisting of Fe–Co enriched precipitates in an Al–Ni enriched matrix produced by spinodal decomposition [46]. Here again, the Fe–Co enriched clusters in the paramagnetic phase are expected to possess strong FM SRO, and since they are embedded in a weakly magnetic Al–Ni matrix, the magnetic origin of spinodal decomposition offers a straightforward explanation of this phenomenon.

Acknowledgments

This work was supported by the Slovenian Research and Innovation Agency (Research Core Fundings No. P1-0125 and P1-0175), the Slovak Research and Development Agency (Grant No. APVV-20-0124), and the Slovak Scientific Grant Agency VEGA (Grant No. 1/0692/22).

Funding

The Javna Agencija za Raziskovalno Dejavnost RS (P1-0125, P1-0175), the Agentúra na Podporu Výskumu a Vývoja (APVV-20-0124), the Vedecká Grantová Agentúra MŠVVaŠ SR a SAV (1/0692/22).

Conflict of Interest

The authors declare no conflicts of interest.

Data Availability Statement

The data that support the findings of this study are available from the corresponding author upon reasonable request.

References

1. B. S. Murthy, J. W. Yeh, and S. Ranganathan, *High-Entropy Alloys* (Elsevier, 2014). 154–155.

2. J.-W. Yeh, S.-K. Chen, H. C. Shih, et al., Functional Properties, *High-Entropy Alloys: Fundamentals and Applications* (Springer International Publishing Switzerland, 2016). 243–248.

3. M. H. Tsai, "Physical Properties of High Entropy Alloys," *Entropy* 15 (2013): 5338–5345.

4. Y. Zhang, T. Zuo, Y. Cheng, and P. K. Liaw, "High-Entropy Alloys With High Saturation Magnetization, Electrical Resistivity, and Malleability," *Scientific Reports* 3 (2013): 1455.

5. T. T. Zuo, M. Zhang, P. K. Liaw, and Y. Zhang, "Novel High Entropy Alloys of FexCo1-xNiMnGa with Excellent Soft Magnetic Properties," *Intermetallics* 100 (2018): 1–8.

6. Y. Zhang, M. Zhang, D. Li, et al., "Compositional Design of Soft Magnetic High Entropy Alloys by Minimizing Magnetostriction Coefficient in (Fe0.3Co0.5Ni0.2)100−x(Al1/3Si2/3)x System," *Metals* 9 (2019): 382.

7. P. Koželj, S. Vrtnik, A. Jelen, et al., "Discovery of a FeCoNiPdCu High-Entropy Alloy With Excellent Magnetic Softness," *Advanced Engineering Materials* 21, no. 1 (2019): 801055.

8. L. Han, Z. Rao, I. R. Souza Filho, et al., "Ultrastrong and Ductile Soft Magnetic High-Entropy Alloys via Coherent Ordered Nanoprecipitates," *Advanced Materials* 33 (2021): 2102139.

9. P. P. Luzar, M. Drienovský, S. Vrtnik, et al., "Zero-Magnetostriction Magnetically Soft High-Entropy Alloys in the AlCoFeNiCux (x = 0.6-3.0) System for Supersilent Applications," 9 (2022): 2201535. Advanced Materials Interfaces

10. L. Han, F. Maccari, I. R. Souza Filho, et al., "A Mechanically Strong and Ductile Soft Magnet With Extremely Low Coercivity," *Nature* 608 (2022): 310–316.

11. M. Harivandi, M. Malekan, and S. A. Seyyed Ebrahimi, "2022):556–564.28(Soft Magnetic High Entropy FeCoNiCuMn Alloy With Excellent Ductility and High Electrical Resistance," *Metals and Materials International*

12. P. Kumari, A. K. Gupta, R. K. Mishra, M. S. Ahmad, and R. R. Shahi, "A Comprehensive Review: Recent Progress on Magnetic High Entropy Alloys and Oxides," *Journal of Magnetism and Magnetic Materials* 554 (2022): 169–142.

13. P. Koželj, A. Jelen, G. Dražić, et al., "Complex Magnetism of Single-Crystalline AlCoCrFeNi Nanostructured High-Entropy Alloy," *iScience* 26 (2023): 106894.

14. W. Gao, Y. Dong, X. Jia, et al., "Novel CoFeAlMn High-Entropy Alloys With Excellentsoft Magnetic Properties and High Thermal Stability," *Journal of Materials Science & Technology* 153 (2023): 22–31.

15. J. Zhu, M. Lv, C. Liu, X. Tan, and H. Xu, "Effect of Neodymium and Yttrium Addition on Microstructure and DC Soft Magnetic Property of Dual-Phase $FeCoNi(CuAl)_{0.8}$ High-Entropy Alloy," *Journal of Rare Earths* 41 (2023): 1562–1567.

16. J. Luzar, A. Jelen, J. Nálepka, et al., "Nanostructure-Induced Functional Combination of Vanishing Magnetostriction and Magnetic Softness in Ferromagnetic $(GaNi)_xCoCrFe$ (x = 0.4-1.6) High-Entropy Alloys," *Materials & Design* 247 (2024): 113396.

17. D. Jiang, Z. Yuan, Z. Zhu, and M. Yao, "NiCoCrFeY High Entropy Alloy Nanopowders and Their Soft Magnetic Properties," *Materials* 17 (2024): 534.

18. A. Kovács, N. B. Venkataraman, V. Chaudhary, et al., "Role of Heterophase Interfaces on Local Coercivity Mechanisms in the Magnetic Al0.3CoFeNi Complex Concentrated Alloy," *Acta Materialia* 246 (2023): 118672.

19. V. Chaudhary, V. Soni, B. Gwalani, R. V. Ramanujan, and R. Banerjee, "Influence of Non-Magnetic Cu on Enhancing the Low Temperature Magnetic Properties and Curie Temperature of FeCoNiCrCu(x) High Entropy Alloys," *Scripta Materialia* 182 (2020): 99–103.

20. V. Chaudhary, R. Chaudhary, R. Banerjee, and R. V. Ramanujan, "Accelerated and Conventional Development of Magnetic High Entropy Alloys," *Materials Today* 49 (2021): 231–252.

21. M. Feuerbacher, "Dislocations and Deformation Microstructure in a B2-Ordered $Al_{28}Co_{20}Cr_{11}Fe_{15}Ni_{26}$ High-Entropy Alloy," *Scientific Reports* 6 (2016): 29700.

22. Q. Lan, A. Kovács, J. Caron, et al., Highly Complex Magnetic Behavior Resulting From Hierarchical Phase Separation in AlCo(Cr)FeNi High-Entropy Alloys, 25(2022):104047.*iScience*

23. A. Manzoni, H. Daoud, R. Völkl, U. Glatzel, and N. Wanderka, "Phase Separation in Equiatomic AlCoCrFeNi High-Entropy Alloy," *Ultramicroscopy* 132 (2013): 212–215.

24. V. Chaudhary, B. Gwalani, V. Soni, R. V. Ramanujan, and R. Banerjee, "Influence of Cr Substitution and Temperature on Hierarchical Phase Decomposition in the AlCoFeNi High Entropy Alloy," *Scientific Reports* 8 (2018): 15578.

25. A. Jelen, P. Koželj, D. Gačnik, et al., "Collective Magnetism of a Single-Crystalline Nanocomposite FeCoCrMnAl High-Entropy Alloy," *Journal of Alloys and Compounds* 864 (2021): 158115.

26. J. M. D. Coey, *Magnetism and Magnetic Materials* (Cambridge University Press, 2010). 299–301.

27. J. S. Langer, "Theory of Spinodal Decomposition in Alloys," *Annals of Physics* 65 (1971): 53–86.

28. D. D. Vvedensky and, *Transformations of Materials* (Morgan & Claypool, 2019). 4-1–4-27.Spinodal Decomposition,

29. D. A. Porter and K. E. Easterling, *Phase Transformations in Metals and Alloys* 2nd (Taylor & Francis, 1992) 263–382. Diffusional transformations in solids.

30. S. Maiti and W. Steurer, "Structural-Disorder and Its Effect on Mechanical Properties in Single-Phase TaNbHfZr High-Entropy Alloy," *Acta Materialia* 106 (2016): 87–97.

31. S. Vrtnik, P. Koželj, A. Meden, et al., "Superconductivity in Thermally Annealed Ta-Nb-Hf-Zr-Ti High-Entropy Alloys," *Journal of Alloys and Compounds* 695 (2017): 3530–3640.

32. A. Takeuchi and A. Inoue, "Classification of Bulk Metallic Glasses by Atomic Size Difference, Heat of Mixing and Period of Constituent Elements and Its Application to Characterization of the Main Alloying Element," *Materials Transactions* 46 (2005): 2817–2829.

33. F. R. de Boer, R. Boom, W. C. M. Mattens, A. R. Miedema, and A. K. Niessen, *Cohesion in Metals: Transition Metal Alloys* (1988). Cohesion and Structure.

34. N. Saunders and A. P. Miodownik, *CALPHAD (Calculation of Phase Diagrams): A Comprehensive Guide, Pergamon Materials Series*. (Elsevier Science & Technology Books, 1998), 229–256.

35. T. Nishizawa, "Progress of CALPHAD," *Materials Transactions, JIM* 33 (1992): 713–722.

36. W. Xiong, Q. Chen, P. A. Korzhavyi, and M. Selleby, "An Improved Magnetic Model for Thermodynamic Modelling," *Calphad* 39 (2012): 11–20.

37. C. A. Schneider, W. S. Rasband, and K. W. Eliceiri, "NIH Image to ImageJ: 25 Years of Image Analysis," *Nature Methods* 9 (2012): 671–675.

38. B. S. Murthy, J.-W. Yeh, and S. Ranganathan, High-Entropy Alloys (Elsevier, 2014). 92.

39. J. M. D. Coey, *Magnetism and Magnetic Materials* (Cambridge University Press, 2010). 209–218.

40. O. Schneeweiss, M. Friák, M. Dudová, et al., "Magnetic Properties of the CrMnFeCoNi High-Entropy Alloy," *Physical Review B: Condensed Matter and Materials Physics* 96 (2017): 014437.

41. D. Ma, B. Grabowski, F. Koermann, J. Neugebauer, and D. Raabe, "*Ab initio* Thermodynamics of the CoCrFeMnNi High Entropy Alloy: Importance of Entropy Contributions Beyond the Configurational One," *Acta Materialia* 100 (2015): 90–97.

42. D. A. Porter and K. E. Easterling, Diffusion, *Phase Transformations in Metals and Alloys* 2nd (Taylor & Francis, 1992), 60–110.

43. C. Niu, A. J. Zaddach, A. A. Oni, et al., "Spin-Driven Ordering of Cr in the Equiatomic High Entropy Alloy NiFeCrCo," *Applied Physics Letters* 106 (2015): 161906.

44. P. Klaver, R. Drautz, and M. W. Finnis, "Magnetism and Thermodynamics of Defect-free Fe-Cr Alloys," *Physical Review B* 74 (2006): 094435.

45. Z. Rao, B. Dutta, F. Körmann, et al., "Beyond Solid Solution High-Entropy Alloys: Tailoring Magnetic Properties via Spinodal Decomposition," *Advanced Functional Materials* 31 (2021): 2007668.

46. W. G. Chu, W. D. Fei, X. H. Li, D. Z. Yang, and J. L. Wang, "Evolution of Fe-Co Rich Particles in Alnico 8 Alloy Thermomagnetically Treated at 800°C," *Materials Science and Technology* 16 (2000): 1023–1028.